

Received:
25 November 2016
Revised:
20 May 2017
Accepted:
27 September 2017

Cite as: Shrok Allami,
Zainab D. Abid Ali, Ying Li,
Hayder Hamody,
Basher Hasan Jawad, Li Liu,
Tianshu Li.
Photoelectrochemical
performance of N-doped ZnO
branched nanowire
photoanodes.
Heliyon 3 (2017) e00423.
doi: [10.1016/j.heliyon.2017.e00423](https://doi.org/10.1016/j.heliyon.2017.e00423)



Photoelectrochemical performance of N-doped ZnO branched nanowire photoanodes

Shrok Allami^{a,*}, Zainab D. Abid Ali^a, Ying Li^b, Hayder Hamody^a,
Basher Hasan Jawad^a, Li Liu^b, Tianshu Li^b

^a Renewable Energy Directory, Ministry of Science and Technology, Baghdad, Iraq

^b Corrosion and Protection Division, Institute of Metal Research, Shenyang, China

* Corresponding author.

E-mail address: shrokabdullah@yahoo.com (S. Allami).

Abstract

A ZnO branched-nanowire (BNW) photoanode was doped with N for use in a photoelectrochemical cell (PEC) to generate H₂ from water splitting. First, ZnO BNWs were synthesized by chemical bath deposition method. Two experimental methods were used for N-doping: the time-controlled direct-current glow discharge plasma (DCGDP) and the DC magnetron plasma (DCMP) methods, to optimize N-doping of the NW structure. X-ray photoelectron spectroscopy (XPS) provided the N distribution and atomic percentage in the BNWs. The XPS results confirmed that N distribution into ZnO BNWs occurred by N substitution of O sites in the ZnO structure and through well-screened molecular N₂. The morphologies and structures of the fabricated nanostructures were investigated by field-emission scanning electron microscopy and X-ray diffraction respectively. The photoanode performance was demonstrated in photoelectrochemical studies at various power densities under both dark and illuminated conditions. Increasing the N amount in the ZnO BNWs increased the photocurrent in the PEC.

Keywords: Engineering, Condensed matter physics, Nanotechnology, Materials science

1. Introduction

The search for efficient and low-cost energy carriers has recently alerted scientists to the promising approach of directly converting solar energy into H₂ [1, 2, 3]. This approach focuses on the production of H₂ from renewable energy resources, using photoelectrochemical cells (PECs) to split water [1, 2, 3]. PECs are solar cells comprising redox media and photoelectrodes fabricated from different materials [4, 5, 6, 7, 8]. The photoelectrode material type and structure are critical in determining the PEC performance [9]. Semiconducting photoanodes in PECs dominate the process of converting incident photons into electron–hole pairs [10]. This conversion and its effects on the water-splitting mechanism were explained in our previous work [11]. A semiconductor with a band gap of 1.6–2.2 eV was ideal for a photoelectrode that could absorb a wide range of the solar spectrum and convert incident photons into electron–hole pairs efficiently [10].

Since the first PEC demonstration with a TiO₂ photoelectrode [4, 5, 6, 7, 8], different nanostructured materials have been studied extensively. Nanostructured metal oxides as photoelectrodes have many advantages, including large surface-area-to-volume ratios, short lateral diffusion lengths for charge carriers, and low reflectivity. Photoelectrodes of Ta₃N₅ in both thin-film and nanoparticle forms have been demonstrated for PEC water splitting [11, 12, 13]. A vertically aligned Ta₃N₅ nanorod photoelectrode yielded a more efficient photocurrent density than a planar Ta₃N₅ anode [13].

A vertically aligned ZnO nanorod array was developed and doped with N via thermal annealing to improve light absorption in the visible region, photocurrent, photon-to-H₂ conversion, and water-splitting efficiency [14]. A heterogeneous 3D branched nanorod photoelectrode was constructed with a p-Si nanowire (NW) core and branches of ZnO NWs with high surface-area-to-volume ratios. This structure was employed to study the effect of surface morphology on the photoelectrochemical water-splitting efficiency. Larger ZnO NW branches and longer, denser p-Si NW cores promoted higher photocathode currents and better efficiency [15].

In this work, ZnO branched NWs (BNWs) were synthesized as a PEC photoelectrode by a chemical bath deposition in order to increase the nanostructure surface-area-to-volume ratio. The structure was then doped with N by time-controlled direct-current (DC) glow-discharge plasma (DCGDP) and DC magnetron plasma (DCMP) methods. The electronic structure, N depth profile, and distribution into ZnO with treatment time were studied via X-ray photoelectron spectroscopy (XPS) results. The effect of the modified electronic structure on the conversion efficiency of solar photons to electron–hole pairs via the flat band potential and photocurrent induced during photoelectrochemical measurement were demonstrated. The aim of this work was to optimize N-doping of ZnO BNWs by controlling the plasma treatment time and to demonstrate the effect of this

doping on the photoresponse, electrochemical properties, and H₂ generation efficiency.

2. Experimental

The ZnO nanostructure was synthesized on a Si (100) wafer substrate by chemical bath deposition process using a nutrient solution of a 1:2 ratio of Zn(NO₃)₂ to hexamethylenetetramine (HMTA) with a pH of 8, under NH₄OH addition at 85 °C for 4 h [16]. The Si wafer was cleaned by dipping in a piranha solution (H₂SO₄:H₂O₂ = 4:1) for 10 min and then in a diluted HF solution (HF: H₂O = 1:100) for 2 min to remove organic impurities and native oxide, respectively. A 20-nm Ti thin film was deposited before a 50-nm-thick layer of Au on the Si wafer by ion beam evaporation. Then, the substrate was annealed at 300 °C for 30 min under Ar. All the chemicals were reagent-grade from Sigma-Aldrich. The substrates were placed face-down at the nutrient solution surface. By surface tension, the substrate floated on the solution surface. The growth of ZnO NWs was conducted in a convection oven. Two categories of N₂ plasma treatments were held at 450 DC V and 100 watt via DCGDP and DCMP for different periods in homemade plasma system, under constant argon environment. The morphologies of the fabricated nanostructures were examined by scanning electron microscopy (SEM, Philips XL30FEG, FEI Co., Hillsboro, OR, USA) with an accelerating voltage of 20 kV. Their structures were analyzed by X-ray diffraction (XRD, Philips diffractometer, PW 1700) with Cu K α radiation, operated at 40 kV and 40 mA. The N concentration and distribution in the ZnO BNWs were quantitatively characterized by XPS (ESCALAB250 X-ray photoelectron spectrometer) using monochromatic Al K α (1486.6 eV) radiation. The binding energy scale was calibrated to an Au 4f_{7/2} line position of 83.98 eV. Ultra-thin depth profiling was conducted by Ar ion bombardment with the ion energy of 2 keV. The measured sample current during depth profiling was 2 mA, and the bombardment area measured 2 mm \times 2 mm. The peak identification was achieved with reference to an XPS database. Photoelectrochemical measurements were performed in a 0.25-M Na₂SO₄ aqueous electrolyte using Pt and Ag/AgCl as the counter and reference electrodes, respectively. Measurements of the dark current and photocurrent under white light at powers of 180 and 250 mW/cm² were performed using linear-sweep polarization (PAR2273 Electrochemical Measurement System, EG&G). The flat band potential at the NW/electrolyte interface was determined by the electrochemical impedance method using Mott–Schottky plotting. Each type of electrochemical measurement was repeated at least three times. The H₂ generation efficiency was measured by steady-state current measurements.

3. Results and discussion

The synthesis of ZnO BNWs was achieved with the addition of NH₄OH as described previously, with results [16], shown in Fig. 1a. Growth advancement

analyzed via XRD patterns clearly explains the changes in the growth directions with time. The phenomenon is depicted in Fig. 1b.

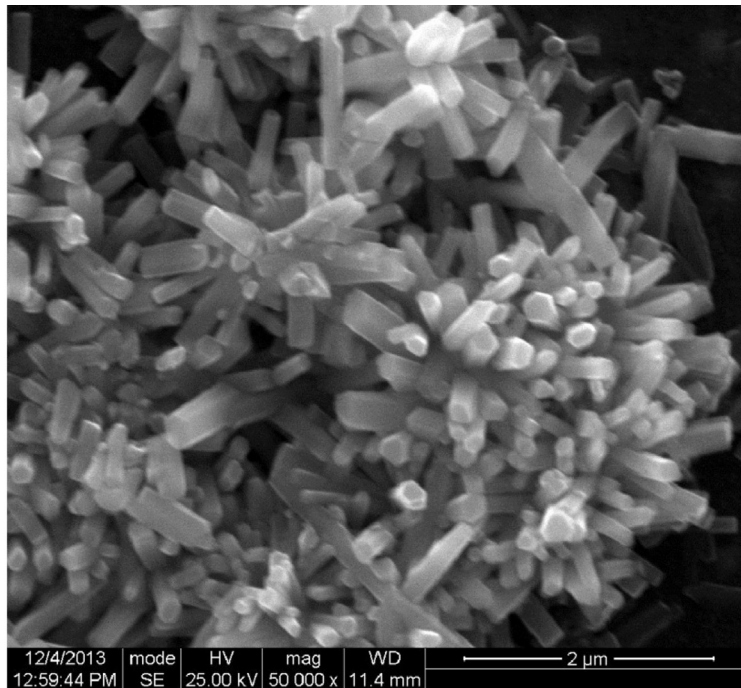
Fig. 2 shows the indexing of the XRD patterns for the ZnO BNWs before and after plasma nitriding, which show a new peak at $2\theta = 32.986^\circ$ related to N_2 , according to the International Centre for Diffraction Data (ICDD) card number 23-1293. The N_2 source may be the room environment. A configuration of XRD with XPS is discussed later.

Plasma treatments affect the NW surface morphology by etching under long treatment periods in DCGDP or by exposure to high-energy ion bombardment in DCMP. Therefore, we used low-energy plasma at 100 W in DCMP for 2, 3, and 4 min and 450-V DCGDP for different periods.

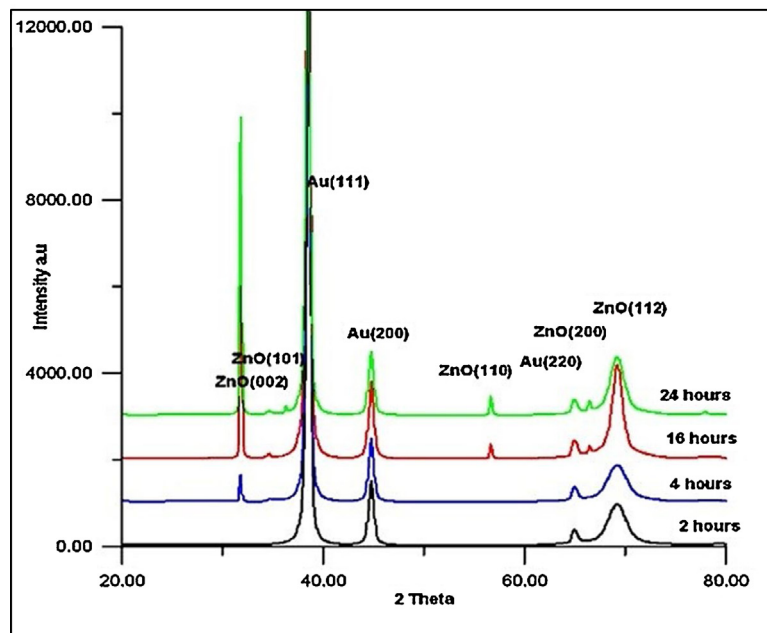
The N incorporated in the ZnO lattice structure with multiple chemical states includes the well-screened molecular state ($\alpha-N_2$), molecular nitrogen ($\gamma-N_2$), ($\alpha-N$) atoms occupying O sites to form Zn_3N_2 [17], $ZnO_{1-x}N_x$ that forms by the decomposition of Zn_3N_2 and the rearrangement of N atoms in the ZnO lattice [17], and NO_2 . The chemical states and bonding energies of these states differ according to the plasma treatment type, as listed in Table 1. As an example of XPS narrow scanning, Fig. 3 shows the binding energies of N 1s for the ZnO BNWs treated by DCMP for 3 min. The appearance of $\gamma-N_2$ in the samples treated by DCMP can be explained by plasma dissociation mechanisms. In a plasma environment, dissociation and recombination occur simultaneously; the process that becomes prevalent depends on the plasma power. The magnetron effect attracting certain species toward the substrate in DCMP increases the appearance opportunity of different N molecules compared to that in DCGDP.

The N concentrations, referring to the atomic ratio of N to Zn in the NWs, can also be determined by XPS analysis. Table 2 shows the increase in N atomic percentage with increasing plasma treatment time; N reaches the maximum percentage of 25.0771% after 100 min and 14.123% after 3 min for DCGDP and DCMP treatments, respectively. Moreover, the depth of N from the DCGDP-treated ZnO NW surfaces is decreased with treatment time until reaching a plateau of 7 nm, after 30 min. The N depth in DCMP-treated ZnO NWs is dramatically decreased with time. This is related to surface etching from the long-term exposure to ion bombardment in the plasma environment of DCGDP and to high-energy ions in DCMP. Fig. 4 shows the highly etched surface morphology of the 4-min DCMP-treated ZnO BNW; the etching is from high-energy ionic bombardment. We neglected to characterize BNW arrays showing significant etching.

Electrochemical impedance measurements for the N-doped ZnO BNW were performed in darkness using Mott–Schottky plots [18] in order to determine the flat band potential V_{fb} . V_{fb} assists in understanding the effects of electronic structure



a



b

Fig. 1. (a). SEM image of branched ZnO NWs. (b). XRD patterns for branched ZnO NWs at different growth periods. More information can be found at Al-lami et al., 2014 [16].

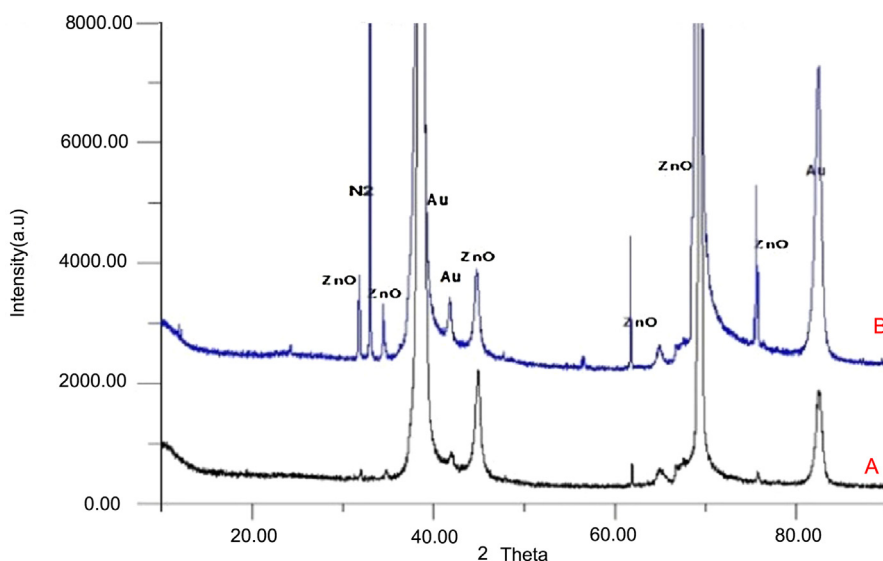


Fig. 2. XRD patterns for (a). ZnO BNWs before plasma treatment, (b). ZnO BNWs after plasma treatment.

changes induced by N-doping of the ZnO BNW on the ZnO/electrolyte interface electrochemistry. For the water-splitting reaction to proceed, V_{fb} of the photoelectrode used in PEC should be more cathodic than the H_2 reduction potential (E_h) of the electrolyte [14]. E_h varies as a function of pH value, quantified by the equation $E_h = 0 - 0.059(\text{pH})$. For our redox electrolyte, E_h is -0.2475 V. For the two categories of plasma treatment samples, V_{fb} becomes more negative with increasing N atomic concentration in the ZnO BNW. The N atoms increase the charge-carrier density in the space charge region and induce new intermediate energy levels in the band gap [19, 20]. These effects decrease the potential required to induce zero charges at the semiconductor redox interface and therefore V_{fb} . Table 3 shows V_{fb} according to plasma treatment type, treatment time, and N concentration.

More cathodic V_{fb} , the maximum N atomic concentration, and the depth results were considered for the next photoelectrochemical tests. Photoelectrodes treated for 100, 160, and 3 min by DCGDP and DCMP, respectively, were chosen. To

Table 1. Binding energies for N 1s chemical states in ZnO BNW.

| Binding energy (eV) | $\alpha\text{-N}_2$ | $\beta\text{-N}$ | $\gamma\text{-N}_2$ | $\text{ZnO}_{1-x}\text{N}_x$ | NO_2 |
|---------------------|---------------------|------------------|---------------------|------------------------------|---------------|
| DCGDP | 397.2 and 404.1 | 396.4 | – | 398.1 | – |
| DCMP | 397.5 and 404.3 | 396.4 | 400.6 | 398.4 & 398.5 | 403.6 |

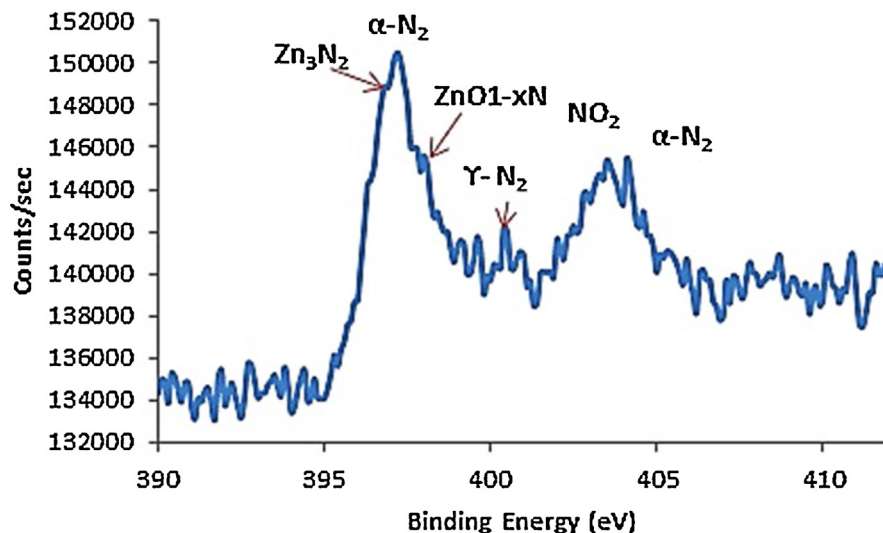


Fig. 3. XPS spectrum for ZnO BNW N_2 plasma-treated by DCMP.

evaluate the properties of the photoanodes in a PEC, linear sweep polarization was conducted both in darkness and under illumination. In dark conditions, almost no current is observed from all plasma-treated ZnO BNW photoanodes. With illumination, the tested photoelectrodes reveal slight increases in photoanodic currents with increasing applied potential and light power density, as illustrated in Fig. 5. SEM images are included depicting each electrode after plasma treatment and before linear polarization testing.

The photocurrent of the N-doped ZnO BNW electrodes is increased with N concentration, as shown in Fig. 5a and 5b. Increasing the N atoms substituting at O sites in the ZnO crystal lattice to form nitrides, as shown by the XPS results, increases the number of intermediate energy levels created in the band gap. This decreases the required photon energy to generate electron-hole pairs, increases

Table 2. N 1s atomic percentages and diffusion depths into ZnO versus plasma treatment time from XPS results.

| Plasma treatment type | Treatment time (min) | N (%) | Depth (nm) |
|-----------------------|----------------------|---------|------------|
| DCGDP | 10 | 13.3255 | 10.0046 |
| DCGDP | 30 | 13.5959 | 7.232 |
| DCGDP | 100 | 25.0771 | 7.512 |
| DCGDP | 160 | 14.1816 | 6.167 |
| DCMP | 2 | 10.7269 | 28.107 |
| DCMP | 3 | 14.123 | 18.046 |

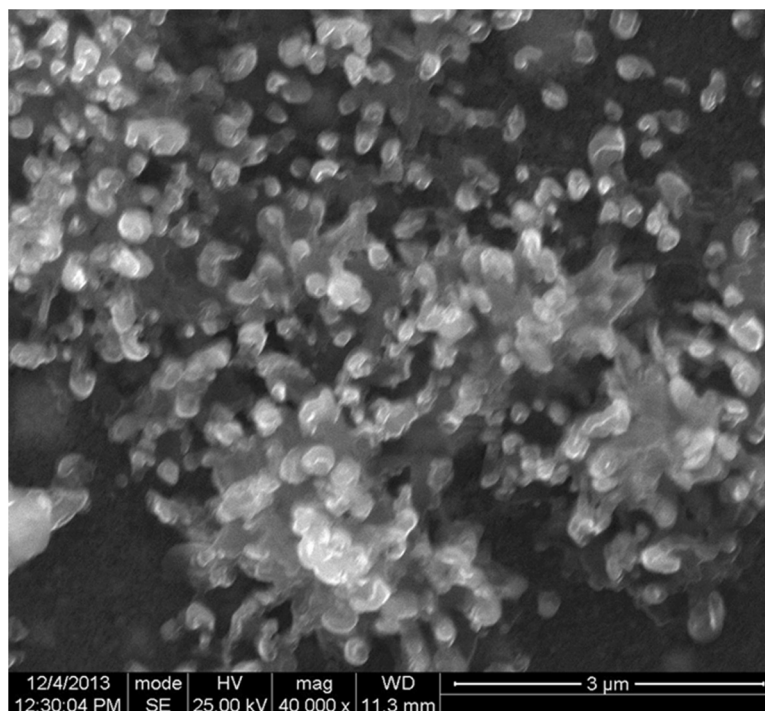


Fig. 4. Highly etched ZnO BNW from exposure to high-energy ions after 4 min DCMP treatment.

electron mobility in the ZnO BNW, decreases electrical resistance, and an increases electron transfer efficiency [21, 22].

In addition, the maximum photoanodic current at 0.8 V applied potential for the DCGDP-treated ZnO BNW electrodes depends on the N concentration, as listed in Table 4. The photoanodic current for the ZnO BNW electrode treated for 3 min by DCMP is higher than that for the electrode treated by DCGDP for 160 min, despite their similar N contents. This may relate to the N depth and states identified by XPS. For ZnO with an N concentration gradient to the surface, the gradient can

Table 3. V_{fb} vs. standard hydrogen electrode (SHE) according to plasma treatment type, time, and N concentration.

| Plasma treatment type | Treatment time (min) | Flat band potential (V_{fb}) vs. SHE (V) | N (%) |
|-----------------------|----------------------|--|---------|
| DCGDP | 10 | -0.2246 | 13.3255 |
| DCGDP | 30 | -0.235424 | 13.5959 |
| DCGDP | 100 | -0.2895 | 25.0771 |
| DCGDP | 160 | -0.26328 | 14.1816 |
| DCMP | 2 | -0.454 | 10.7269 |
| DCMP | 3 | -0.46311 | 14.123 |

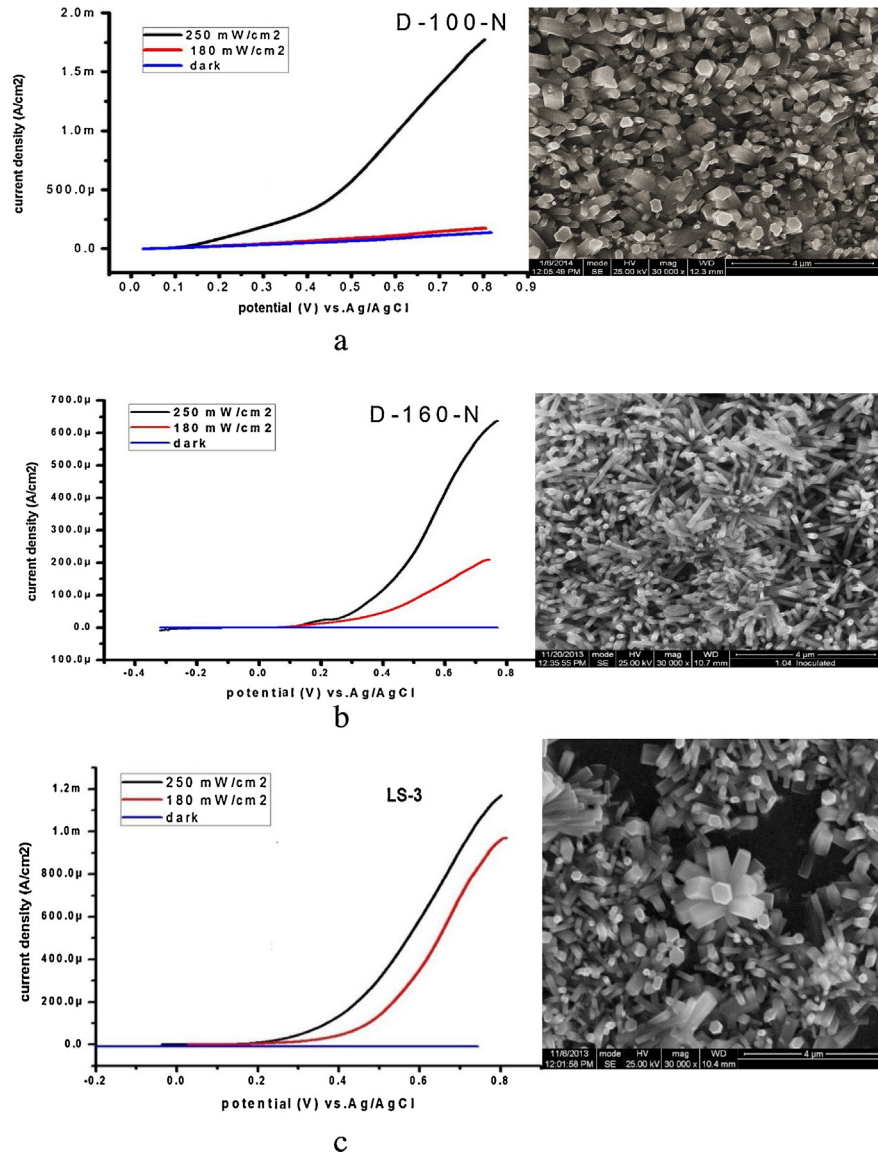


Fig. 5. Linear-sweep polarization measurements for ZnO BNW photoanode treated for (a). 100 min, (b). 160 min by DCGDP, and (c). 3 min by DCMP.

Table 4. Comparison of the effect of plasma treatment type on N concentration and depth on the photoanodic current at 0.8 V under the illumination power of 250 mW/cm².

| Plasma treatment type | V_{fb} (V) | N (%) content of ZnO BNW | N depth surface (nm) | Photoanodic current (mA) |
|-----------------------|--------------|--------------------------|----------------------|--------------------------|
| DCGDP 100 min | -0.2895 | 25.0771 | 7.512 | 1.7 |
| DCGDP 160 min | -0.26328 | 14.1816 | 6.167 | 0.637 |
| DCMP 3 min | -0.46311 | 14.123 | 18.046 | 1.17 |

Table 5. Comparison of previous research results.

| Ref | Result | N doping technique | Notes |
|------|---|------------------------------|---|
| [23] | $\sim 160 \mu\text{A}/\text{cm}^2$ at 1.1 V | Different implantation doses | wurtzite structure ZnO, diameter ranging from 60 nm to 120 nm and length of ca. 3 μm |
| [14] | $400 \mu\text{A}/\text{cm}^2$ at +1.0 V | Annealing in ammonia | <0002> wurtzite structure, diameter (80–130 nm) with typical NW lengths of 1–2 μm |
| [15] | $\sim 0.5 \text{mA}/\text{cm}^2$ at +1.5 V | Without doping | Average ZnO NW lengths of ~ 90 and ~ 200 nm. Diameter 25–30 nm |

efficiently promote photoinduced electron–hole transfer via the terraced band structure [23]. From these results, the N concentrations, depths, and chemical states are critical in determining the photoelectrode's response to photoelectrochemical reactions. A comparison between this work and previous research results is listed in Table 5.

The N doping amount in the ZnO BNW also affects the efficiency of H_2 generation (η') under exposure to photons. The η' values are calculated by the Eq. (1) [20]:

$$\eta' = I (1.23 - V) J \quad (1)$$

Where I is the steady-state current, V the applied potential, and J the power density of the light. The steady-state current values are obtained from transient current density measurements. Steady-state current measurements for the ZnO BNW photoanodes DCGDP-treated for 100 min and DCMP treated for 3 min were performed at $250 \text{mW}/\text{cm}^2$ under a light on/off pattern at 300-s intervals. In Fig. 6, the calculated results of H_2 production efficiency are plotted versus the applied

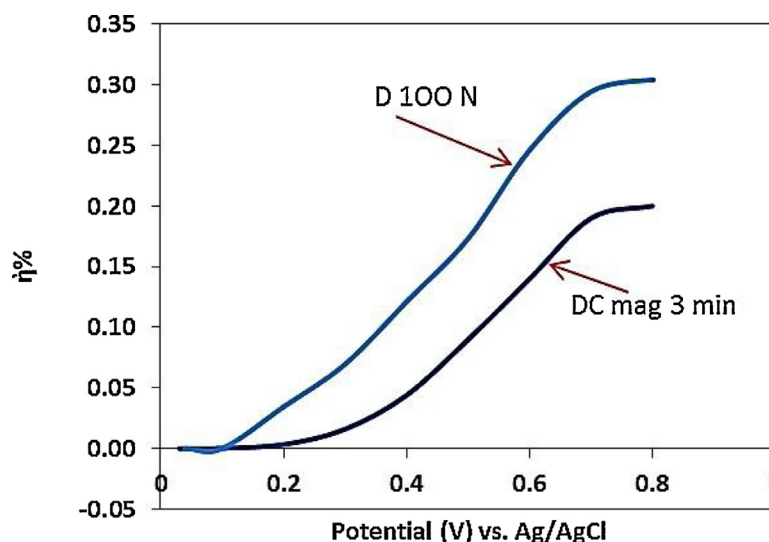


Fig. 6. H_2 production efficiency vs. applied potential for plasma-treated N-doped ZnO BNW photoanode.

potential. The H₂ generation efficiency for the N-doped ZnO anodic electrode treated for 100 min by DCGDP is higher than that for the electrodes treated for 3 min in DCMP throughout the applied potential range. This is because of the higher photocurrent response mentioned above.

4. Conclusion

The synthesis of ZnO BNW is performed chemical bath deposition by tuning of wet-processing parameters, followed by DCGDP and DCMP treatment to dope N into the BNWs. This affects the BNW electrodes in terms of electrochemical impedance, ZnO/electrolyte interface electrochemistry, photoanodic current response, and efficiency in photon-to-H₂ (η) generation. The DCGDP treatment is more appropriate for N-doping of ZnO BNWs than DCMP treatment. This is because the high-energy ion bombardments during DCMP treatment etch the BNW surface, thereby reducing the N concentration and depth.

Declarations

Author contribution statement

Shrok Allami: Conceived and designed the experiments; Performed the experiments; Analyzed and interpreted the data; Wrote the paper.

Zainab D. Abid Ali, Hayder Hamody, Basher Hasan Jawad: Performed the experiments Ying Li: Analyzed and interpreted the data.

Li Liu, Tianshu Li: Contributed reagents, materials, analysis tools or data.

Competing interest statement

The authors declare no conflict of interest.

Funding statement

This research did not receive any specific grant from funding agencies in the public, commercial, or not-for-profit sectors.

Additional information

No additional information is available for this paper.

Acknowledgments

The main author, Shrok Allami, would like to thank all the employees at the State Key Laboratory for Corrosion and Protection, Institute of Metal Research, Chinese Academy of Science for their support. In addition, she would also like to thank her

home institute, the Ministry of Science and Technology, and Renewable Energy Directory for their official and technical support.

References

- [1] M. Grätzel, Photoelectrochemical cells, *Nature* 414 (2001) 338.
- [2] M.G. Walter, E.L. Warren, J.R. McKone, S.W. Boettcher, Q.X. Mi, E.A. Santori, N.S. Lewis, Solar water splitting cells, *Chem. Rev.* 110 (2010) 6446.
- [3] Yasuhiro Tachibana, Lionel Vayssieres, James R. Durrant, Artificial photosynthesis for solar water-splitting, *Nat. Photon.* 6 (2012) 511–518.
- [4] A. Fujishima, K. Honda, Electrochemical photolysis of water at a semiconductor electrode, *Nature* 238 (July) (1972) 37–38.
- [5] Jieyang Jia, Linsey C. Seitz, Jesse D. Benck, Yijie Huo, Yusi Chen, Jia Wei, Desmond Ng, Taner Bilir, James S. Harris, Thomas F. Jaramillo, Solar water splitting by photovoltaic-electrolysis with a solar-to-hydrogen efficiency over 30%, *Nat. Commun.* 7 (2016) 13237.
- [6] R. Abe, Recent progress on photocatalytic and photoelectrochemical water splitting under visible light irradiation, *J. Photochem. Photobiol. C: Photochem. Rev.* 11 (2010) 179.
- [7] K. Sivula, F. Le Formal, M. Grätzel, Solar water splitting: progress using hematite (α -Fe₂O₃) photoelectrodes, *ChemSusChem* 4 (4) (2011) 432–449.
- [8] T. Hisatomi, H. Dotan, M. Stefi k, K. Sivula, A. Rothschild, M. Grätzel, N. Mathews, Enhancement in the performance of ultrathin hematite photoanode for water splitting by an oxide underlayer, *Adv. Mater.* 24 (2012) 2699.
- [9] W. Adrian Bott, Electrochemistry of semiconductors, *Curr. Sep.* 17 (1998) 3.
- [10] Li Yanbo, Tsuyoshi Takata, Dongkyu Cha, Kazuhiro Takanabe, Tsutomu Minegishi, Jun Kubot, Kazunari Domen, Vertically aligned Ta₃N₅ nanorod arrays for solar-driven photoelectrochemical water splitting, *Adv. Mater.* 25 (2013) 125–131.
- [11] D. Yokoyama, H. Hashiguchi, K. Maeda, T. Minegishi, T. Takata, R. Abe, J. Kubota, K. Domen, Ta₃N₅ photoanodes for water splitting prepared by sputtering, *Thin Solid Films* 519 (7) (2011) 2087–2092.
- [12] M. Higashi, K. Domen, R. Abe, Fabrication of efficient TaON and Ta₃N₅ photoanodes for water splitting under visible light irradiation, *Energy Environ. Sci.* 4 (2011) 4138.

- [13] X. Feng, T.J. La Tempa, J.I. Basham, G.K. Mor, O.K. Varghese, C.A. Grimes, Ta₃N₅ nanotube arrays for visible light water photoelectrolysis, *Nano Lett.* 10 (2010) 948.
- [14] Xunyu Yang, Abraham Wolcott, Gongming Wang, Alissa Sobo, Robert Carl Fitzmorris, Fang Qian, Jin Z. Zhang, Yat Li, Nitrogen-doped ZnO nanorods arrays for photoelectrochemical water splitting, *Nano Lett.* 9 (6) (2009) 2331–2336.
- [15] Alireza Kargar, Ke Sun, Yi Jing, Chulmin Choi, Huisu Jeong, Gun Young Jung, Sungho Jin, Deli Wang, 3d branched nanowire photoelectrochemical electrodes for efficient solar water splitting, *ACS Nano* 7 (10) (2013) 9407.
- [16] Shrok Al-lami, Halima Jaber, Controlling ZnO nanostructure morphology on seedless substrate by tuning process parameters and additives, *Chem. Mater. Res.* 6 (4) (2014) 101.
- [17] N. Tabet, M. Faiz, A. Al-Oteibi, XPS study of nitrogen-implanted ZnO thin films obtained by DC-Magnetron reactive plasma, *J. Electron. Spectrosc. Relat. Phenom.* 163 (2008) 15–18.
- [18] K. Gelderman, L. Lee, S.W. Donne, Flat-band potential of a semiconductor: using the Mott–Schottky equation, *J. Chem. Educ.* 84 (4) (2007) 685.
- [19] K. S.Ahn, Y. Yan, S. Shet, T. Deutsch, J. Turner, M. Al-Jassim, Enhanced photoelectrochemical responses of ZnO films through Ga and N codoping, *Appl. Phys. Lett.* 91 (2007) 231909.
- [20] B. Parkinson, On the efficiency and stability of photoelectrochemical devices, *Acc. Chem. Res.* 17 (1984) 431–437.
- [21] K.S. Ahn, Y. Yan, S. Shet, K. Jones, T. Deutsch, J. Turner, M. Al- Jassim, ZnO nanocoral structures for photoelectrochemical cells, *App. Phys. Lett.* 93 (2008) 163117.
- [22] K.S. Ahn, Y. Yan, S.H. Lee, T. Deutsch, J. Turner, C.E. Tracy, C.L. Perkins, M.M. Al-Jassim, Photoelectrochemical Properties of N-Incorporated ZnO Films Deposited by Reactive RF Magnetron Sputtering, *J. Electrochem. Soc.* 154 (9) (2007) B956–B959 238, 37 (1972).
- [23] Meng Wang, Feng Ren, Jigang Zhou, Guangxu Cai, Li Cai, Yongfeng Hu, Dongniu Wang, Yichao Liu, Liejin Guo, Shaohua Shen, N Doping to ZnO Nanorods for Photoelectrochemical Water Splitting under Visible Light: Engineered Impurity Distribution and Terraced Band Structure, *Scientific Reports* 5 (2015) 12925.